Chinese Journal of
POLYMER SCIENCE

RESEARCH ARTICLE

https://doi.org/10.1007/s10118-024-3130-8
Chinese J. Polym. Sci. **2024**, *42*, 936–945

3D Printed Polyimide/Silica Composite Aerogels for Customizable Thermal Insulation from −50 °C to 1300 °C

Dingyi Yu[a], Tiantian Xue[a], Zhuocheng Ma[a], Zaiyin Hu[c], Lijuan Long[d], Yue-E Miao[a], Wei Fan[a,b*], and Tianxi Liu[a,b]

[a] *State Key Laboratory for Modification of Chemical Fibers and Polymer Materials, College of Materials Science and Engineering, Donghua University, Shanghai 201620, China*
[b] *Key Laboratory of Synthetic and Biological Colloids, Ministry of Education, School of Chemical and Material Engineering, Jiangnan University, Wuxi 214122, China*
[c] *Guizhou Aerospace Wujiang Electro-Mechanical Equipment Co., Ltd., Zunyi 563000, China*
[d] *School of Materials and Architectural Engineering, Guizhou Normal University, Guiyang 550025, China*

Electronic Supplementary Information

Abstract Aerogels are widely used as thermal insulation materials because of their high porosity and low bulk density. However, the insulation performance of aerogels is limited to a narrow temperature range. Besides, the preparation of aerogel materials with precisely controlled and complex architectures is still challenging. Here, we report 3D printed polyimide/silica aerogel particle (PI/SAP) composite aerogels for thermal insulation in a wide range of temperature with customized applications. The printability and shape fidelity of 3D printed composite aerogels is improved by adding hydrophilic SAP as a rheology modifier. The resulting PI/SAP composite aerogel exhibits excellent flame-retardant properties and thermal insulation from −50 °C to 1300 °C. Moreover, the PI/SAP composite aerogel with customized shape can be applied for battery insulation at subzero temperatures, promising to be used as customizable and stable insulating materials in a variety of complex and extreme applications.

Keywords 3D printing; Polyimide; Aerogel; Silica; Thermal insulation

Citation: Yu, D. Y.; Xue, T. T.; Ma, Z. C.; Hu, Z. Y.; Long, L. J.; Miao, Y. E.; Fan, W.; Liu, T. X. 3D printed polyimide/silica composite aerogels for customizable thermal insulation from −50 °C to 1300 °C. *Chinese J. Polym. Sci.* **2024**, *42*, 936–945.

INTRODUCTION

With the continuous development of technology and industry, there is an increasing demand for thermal insulation materials, which can maintain excellent thermal insulation performance and flame-retardant effect in high and low-temperature environments.[1–4] While most thermal insulation materials can maintain good thermal insulation performance at low temperatures, their thermal insulation performance decreases seriously with an increase of temperature.[5–7] Additionally, common commercial insulation materials, such as polystyrene foam and polyurethane foam, are flammable and lose insulation ability at elevated temperatures.[8–10] Therefore, it is of great significance to design and develop thermal insulation materials that can maintain excellent thermal insulation and flame-retardant performance in both high and low-temperature environments.

* Corresponding author, E-mail: weifan@dhu.edu.cn
or weifan@jiangnan.edu.cn

Special Issue: Functional Polymer Materials
Received January 12, 2024; Accepted March 28, 2024; Published online May 17, 2024

Aerogel is a solid material with a porous network structure.[11–15] Its low volume density and porous structure make it effective in preventing heat conduction.[16] Hence, compared to traditional thermal insulation materials, aerogels exhibit lightweight and much better insulation capability. As a typical aerogel material, silica aerogels show good flame retardancy, thermal stability, and ultra-low thermal conductivity.[17–20] However, its mechanical brittleness leads to the poor formability and processability, and long-term use can lead to fatigue damage, powder loss and other issues. Recent studies showed that polyimide aerogels exhibit excellent mechanical properties and thermal stability due to the rigid five-membered ring structure in the main chain, as well as excellent thermal insulation performance.[14,15,18,21] The introduction of inorganic fillers can further improve the flame retardancy and thermal insulation of polyimide aerogels.[4,22] Composite aerogels combine the excellent mechanical strength of polyimide and the good thermal stability of inorganic fillers, while maintain their thermal insulation properties at medium to high temperatures. However, current fabrication methods of composite aerogels are limited to mold casting with limited design flexibility, restricting their applica-

tion in specific complex structures.

3D printing technology enables aerogels to achieve complex structural design,[23–27] making it easy to customize the shape to be applied to scenes with precise shape requirements.[28] According to previous work, it is known that the good rheological behavior of the ink, and the curing and drying of the printed product are the key for the preparation of 3D printed aerogels.[29–32] Some studies reported the additive manufacturing of polyimide aerogels, which are mainly prepared by direct ink writing (DIW) or photo-curing.[33–37] However, due to the low printability of the ink, short print window, and shrinkage during the imidization process, the resolution of the product is reduced, and the shape is not accurately replicated. Therefore, it is crucial to add rheological modifiers and skeleton fillers to improve ink properties for stable printability and enhance performance of printed product.

In this work, 3D printed polyimide/silica composite aerogel has been prepared by utilizing poly(amic acid) (PAA) aqueous solution as the base ink and hydrophilic silica aerogel particle (SAP) as the rheological modifier and reinforcement filler. The silicon hydroxyl group on SAP can form hydrogen bonds with the carbonyl group of PAA, which can effectively ensure the uniform dispersion of the filler in the ink and improve the yield stress and modulus of the ink to achieve direct ink writing. The printed PI/SAP composite aerogel exhibits effectively improved mechanical properties, enhanced heat insulation, and improved flame-retardant properties. It maintains low thermal conductivity in medium-high temperature environments and can still maintain its original structure at temperatures of thousands of degrees Celsius. Moreover, the PI/SAP composite aerogel with customized shape can be applied for battery insulation at subzero temperatures, indicating its excellent thermal insulation performance.

EXPERIMENTAL

Preparation of PAA/SAP Inks

According to our previous work, the PAA solution was obtained by condensation polymerization of pyromellitic dianhydride (PMDA) and 4,4′-oxidianiline (ODA) in *N*,*N*-dimethylacetamide.[14,34] Hydrophilic silica aerogel particle (particle size of ~20 μm, pore size of 20 nm) was obtained from Erico New Materials Co., Ltd. SAP was then dispersed in 15 mL of deionized water, followed by the addition of 1.2 g of PAA and 0.5 mL of triethylamine. The mixture was then stirred at 40 °C for complete dissolution and even distribution of SAP. According to the different SAP contents (20, 53 and 120 mg·mL^{-1}), the theoretical content of SAP in the PAA/SAP composite were 20 wt%, 40 wt% and 60 wt%, respectively. Accordingly, the composite inks were named as PAA/SAP-20, PAA/SAP-40 and PAA/SAP-60, respectively.

3D Printing Process and Fabrication of Polyimide/Silica Composite Aerogel

The syringe filled with the PAA/SAP ink was installed on a machine for direct ink writing under a certain programmed path (EFL-BP6601, China). The diameter of needle used in the printing process was 0.4 mm, the air pressure was maintained at 600 kPa, and movement speed of the needle was 4–6 mm·s^{-1}. After printing, the PAA/SAP products obtained from printing were quickly placed in liquid nitrogen atmosphere to be fully frozen, and then put into a freeze dryer for ice crystal sublimation for 72 h to obtain PAA/SAP aerogel products. Finally, the products were thermally imidized in a tube furnace under nitrogen protection at a ramp rate of 2 °C·min^{-1} and held at 100, 200 and 300 °C for 30 min, respectively. Finally, the 3D printed polyimide/silica aerogel particle (PI/SAP) composite aerogels were obtained.

Characterizations

The morphologies of the PI/SAP aerogel frame and silica aerogel particle were investigated by scanning electron microscope (FESEM, JSM-7500F, Japan) and transmission electron microscope (TEM, JEM-2100F, Japan). Rheological properties of PAA/SAP composite inks were tested by a modular compact rheometer (MCR302, Anton Paar, China). Compression and tensile tests were performed using the Electronic Universal Testing Machine (UTM2102, China). In stretch mode: the sensor is 100 N, and the speed is 10 mm·min^{-1}; in compression mode: the sensor is 2 kN at a rate of 10 mm·min^{-1}. The thermal stability of PI/SAP composites was analyzed using a thermogravimetric analyzer (TA Q5000IR) under air atmosphere at the heating rate of 10 °C·min^{-1}. Thermal conductivity is measured by Hot Disk TPS 2500 S instrument (Hot Disk AB, Sweden). Thermographic images were taken by an infrared thermal camera (TiS40, Fluke Co., Ltd., USA). Fourier-transform infrared spectra (FTIR) were recorded with a Nicolet 6700 FTIR spectrophotometer (Bruker Spectrum Instruments, USA). The charge and discharge test of the battery was performed using the New Land battery test system (CT2001A, China), using a current of 4 mA with a voltage range of 2–4.5 V. The commercial ML1220 lithium manganate battery was used in the battery capacity test.

RESULTS AND DISCUSSION

Fabrication of the PI/SAP Aerogel

The preparation process of PI/SAP aerogel is shown in Figs. 1(a) and 1(b). Briefly, SAP and PAA were dispersed in deionized water to obtain uniform PAA/SAP ink (photograph shown in Fig. S1 in the electronic supplementary information, ESI). Then, PAA/SAP inks with different SAP contents were filled into the printing syringes and stacked layer by layer on the platform through an extrusion-based 3D printer. Afterwards, the printed products were frozen in liquid nitrogen atmosphere, and PI/SAP aerogels with thermal insulation properties were finally obtained by subsequent freeze-drying and thermal imidization. The chemical structure of PI/SAP aerogel was analyzed by FTIR spectroscopy (Fig. S2 in ESI). Typical imide ring carbonyl bands appearing at 1776 and 1721 cm^{-1}, combined with the C—N band at 1363 cm^{-1} and the C—N—C bands at 1007 and 736 cm^{-1}, indicated that PAA was completely converted to PI in the composite. A strong absorption band appears at 1095 cm^{-1}, which was attributed to the antisymmetric stretching vibration of Si—O—Si bond,[38,39] indicating the good combination of SAP and PI.

The key premise for DIW is printable ink with proper rheological properties. The presence of silicon hydroxyl groups on SAP can form hydrogen bond with the carbonyl groups on the surface of PAA (FTIR spectra in Fig. S3 in ESI), which effectively ensures good interfacial interaction and forms a stable

https://doi.org/10.1007/s10118-024-3130-8

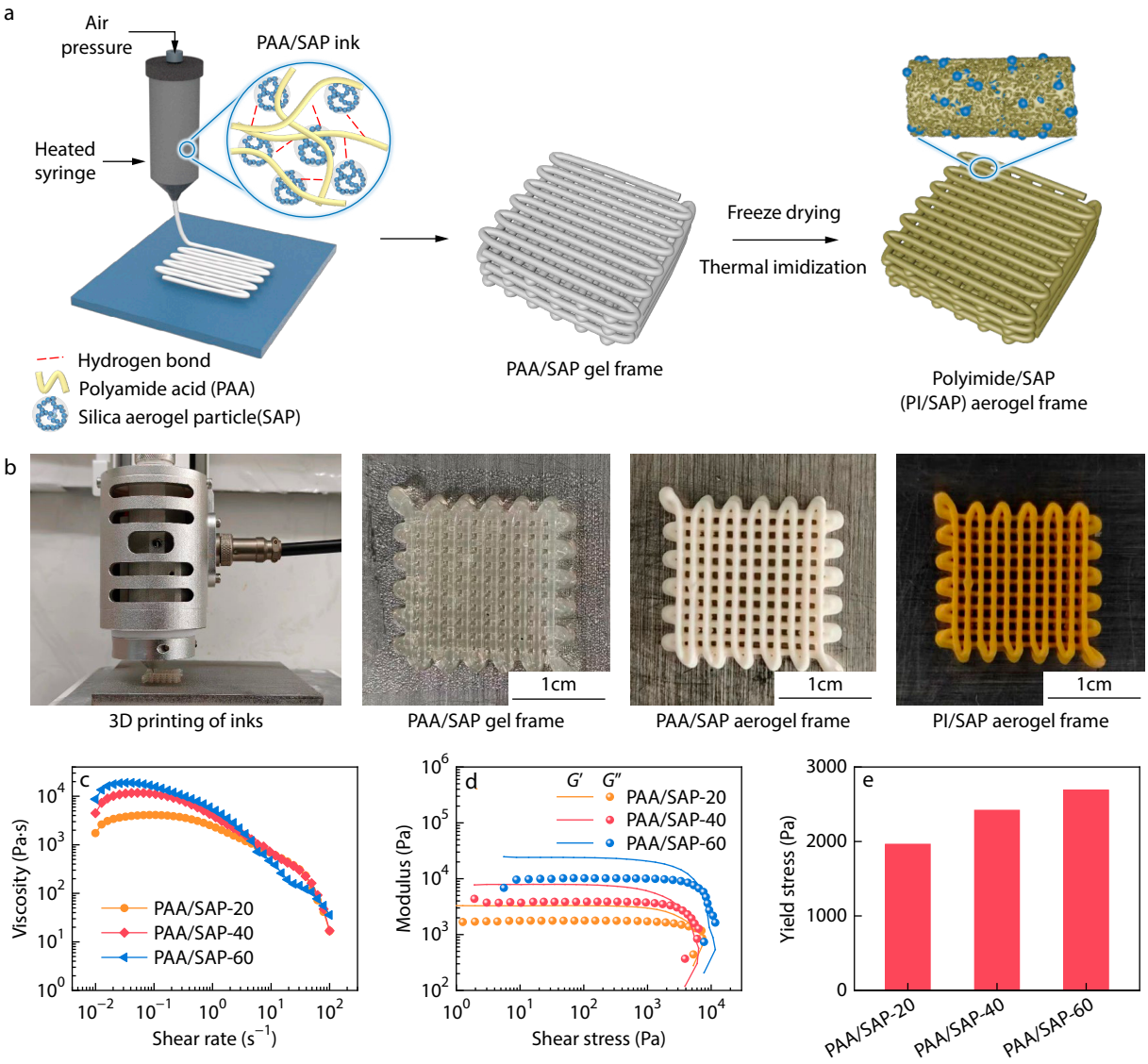

Fig. 1 3D printing of PI/SAP composite aerogels. (a) Schematic illustration of the preparation of PI/SAP composite aerogel; (b) Photographs of 3D printed PI/SAP aerogel frame from inks to aerogels; (c) Steady-state shear viscosity of the PAA/SAP inks; (d) Storage modulus and loss modulus of PAA/SAP inks as a function of shear stress; (e) Yield stress of PAA/SAP inks containing different SAP contents.

three-dimensional network in the solution. From the steady-state shear test (Fig. 1c), it can be observed that with the increase of SAP content, the initial viscosity of the ink increases, and its shear thinning behavior is more obvious, which proves that SAP can significantly improve the extrusion ability of PAA composite ink and help to form a stable and continuous extrusion. In the amplitude scan (Figs. 1d and 1e), the addition of SAP significantly increased the storage modulus from 5000 Pa to 40000 Pa and yield stress from less than 2000 Pa to 2700 Pa of the ink, which could improve the anti-deformation ability of the ink, effectively ensuring the stability of the printed structure. From the rheological results, it can be found that PAA/SAP composite ink has good printability in a wide range of SAP content (20 wt%–60 wt%). Besides, due to the addition of large-size fillers, the movement of polymer molecular chains is limited, thus effectively inhibiting the shrinkage of the products during the freeze-drying and thermal imidization process.

Figs. 2(a)–2(c) show the PI/SAP aerogels with different structures such as frame, maple leaf, and snowflake obtained by 3D printing, which shows the good printability and formability of the composite aerogel. The volume shrinkage of PI/SAP-20 samples during the whole printing process is about 23%, and the volume shrinkage can be reduced to 14% for PI/SAP-60 sample (Fig. 2d). Different from the general fillers, the addition of SAP does not increase the density but reduces the density of the composite aerogel (Fig. 2e). The density of PI/SAP-20 is 0.186 g·mL^{-1}, while the density of the PI/SAP-60 sample is only 0.167 g·mL^{-1}. When the silica content is increased, the skeleton density of the composite aerogel increases while the apparent density decreases, leading to a significant increase in porosity from 87% to about 92%. Therefore, adding SAP as a filler can reduce the shrinkage and improve the porosity of PI/SAP composite aerogels, which

https://doi.org/10.1007/s10118-024-3130-8

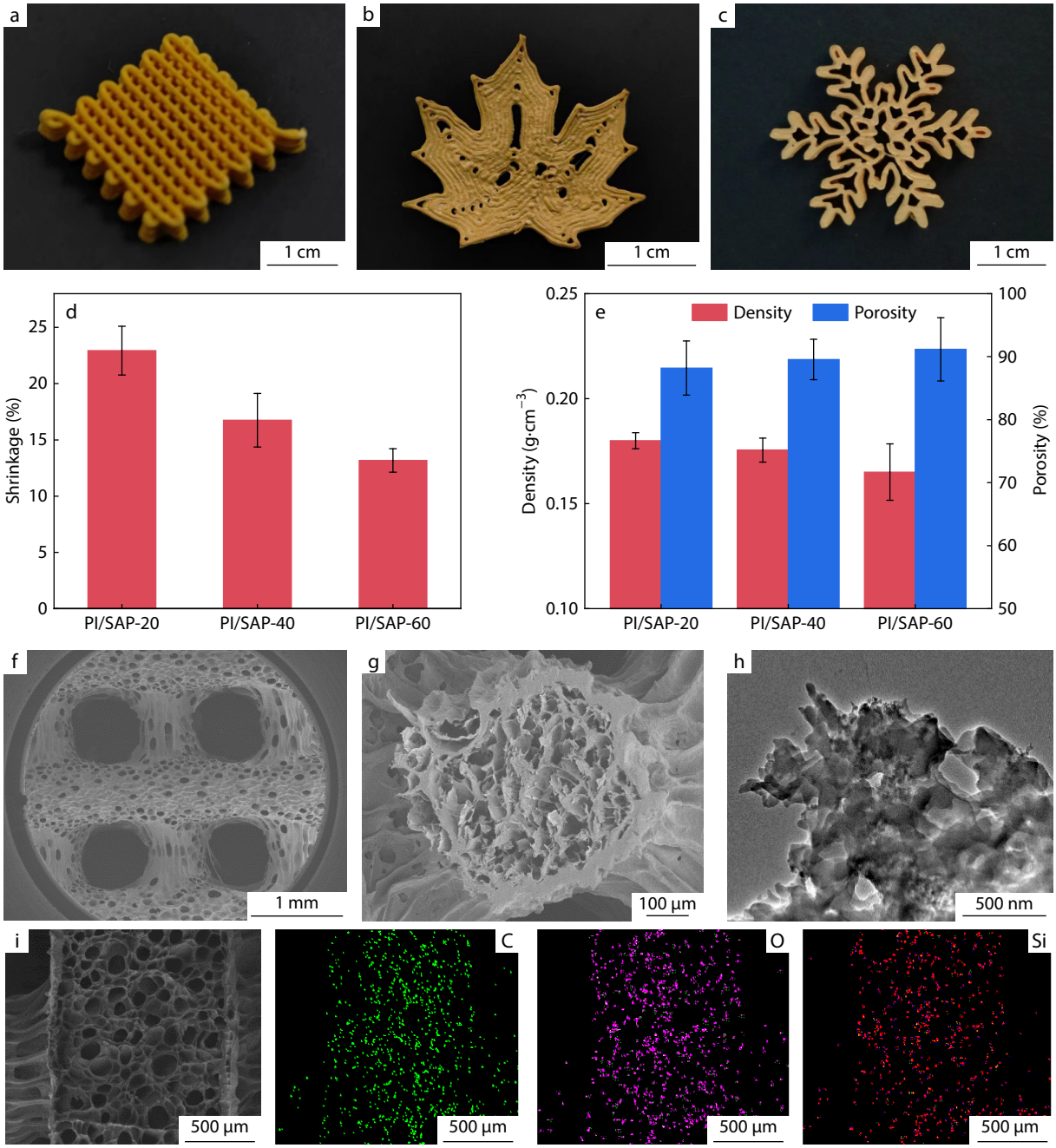

Fig. 2 Morphology and structural characteristics of the PI/SAP aerogel. (a–c) 3D printed PI/SAP aerogel with frame, maple leaf, and snowflake structure; (d) Shrinkage, and (e) density and porosity of 3D printed PI/SAP aerogels with different SAP contents; (f–g) SEM images of PI/SAP-40 aerogel; (h) TEM image of PI/SAP-40 aerogel; (i) SEM-EDS mapping of PI/SAP-40 aerogel.

would effectively ensure the thermal insulation performance of the product.

In order to study the microstructure of printed products, we printed an orthogonal grid structure of PI/SAP aerogel. The grid surface was observed by a low-magnification SEM image (Fig. 2f). It can be observed that the printed frame structure is distinct and has a certain adhesion between adjacent layers, which proves the good interfacial bonding between the adjacent filaments. The cross-sectional SEM image of the filament (Fig. 2g) shows a typical porous structure with pore size of tens of microns, indicating a typical freeze-dried aerogel structure. The silica nanoparticle network in the aerogel can be observed under TEM image in Fig. 2(h). Through elemental analysis of the aerogel (Fig. 2i), it is observed that carbon (C), oxygen (O), and silicon (Si) elements are evenly distributed on the cross-section of the composite aerogel, which further illustrates the good dispersion of SAP in the composite aerogel.

Mechanical and Thermal Properties of Printed PI/SAP Composite Aerogels

The mechanical properties of PI/SAP composite aerogel were

https://doi.org/10.1007/s10118-024-3130-8

evaluated by the compressive stress-strain curves. As shown in Fig. 3(a), the compression process of the composite aerogel is mainly divided into three sections. The first section is the elastic deformation zone below 10% strain, which mainly reflects the deformation resistance of the aerogel skeleton. The second section is the 10%–50% yield section. At this stage, the pore size compression occurs, accompanied by a certain degree of skeleton yield collapse. The higher modulus at this stage means that the skeleton maintains the strength level of the pore structure. In the third section, when the strain is greater than 60%, the pore size is completely collapsed and densified, and the stress is greatly increased, indicating the intrinsic compression performance of the skeleton. When the addition of SAP increased from 20 wt% to 40 wt%, the slope of the initial section of the stress-strain curve increased, demonstrating the higher modulus of PI/SAP-40. Besides, the slope and value of the second section of the curve increased, indicating that the skeleton strength increased enough to maintain the pore structure under compression. When the content of SAP increased to 60 wt%, although it showed a higher modulus, a typical yield platform appeared in the second stage, which indicates an irreversible continuous damage of the pore structure during the compression process.[40] Fig. 3(b) shows that although the modulus of composite aerogel increases gradually with the increase of SAP content (from 8 MPa to 22 MPa), the compressive strength of the PI aerogel is maintained when the addition of SAP is less than 40 wt%. When the SAP content reaches 60 wt%, the compression strength falls off a cliff, indicating the brittle structure of the composite aerogel, which is unfavorable for practical applications.[41] In addition, the compression cycle test of PI/SAP-40 showed that PI/SAP-40 still maintained its maximum stress of 2.9 MPa after compression, and no significant collapse was found in the macroscopic structure, indicating its good mechanical stability (Fig. S4 in ESI).

Due to the intrinsic nanoporous structure of the silica aerogel particles (Figs. S5a and S5b in ESI), thermal conduction in the silica aerogel particles is greatly inhibited. Therefore, unlike general inorganic fillers, silica aerogel particles can further improve the thermal insulation of the composite aerogels at a high addition amount. As shown in Fig. 3(c), the overall thermal conductivity of the aerogel gradually decreases with the increase of SAP content. When the SAP content increased from 20 wt% to 60 wt%, the thermal conductivity of PI/SAP composite aerogels decreased from 59 $mW·m^{-1}·K^{-1}$ to about 44 $mW·m^{-1}·K^{-1}$ at 25 °C (Fig. 3c). Then the thermal conductivity of PI/SAP-40 were tested under different temperatures (Fig. 3d). The thermal conductivity of the PI/SAP-40 aerogel is 42 $mW·m^{-1}·K^{-1}$ at −50 °C. As the temperature rises, the thermal conductivity of PI/SAP-40 increases slightly, and its thermal conductivity is only 81 $mW·m^{-1}·K^{-1}$ at 250 °C, indicating the good thermal insulation properties in a wide range of temperatures. Subsequently, the heat resistance of the composites was evaluated by thermogravimetric analysis in air atmosphere. As shown in Fig. 3(e), the initial thermal decomposition temperature of pure PI aerogel in the air is about 350 °C, while the initial thermal decomposition temperature of PI/SAP-20, PI/SAP-40 and PI/SAP-60 reaches 450, 509 and 516 °C, respectively. In addition, the actual content of SAP in PI/SAP-20, PI/SAP-40 and PI/SAP-60 composite aerogels is 14.3 wt%, 32.4 wt%, and 53.6 wt%, respectively, according to the TGA curves. Therefore, the increase of SAP content can effectively reduce the thermal conductivity and significantly improve the thermal stability of the PI/SAP composite aerogel. With the consideration of mechanical properties, PI/SAP-40

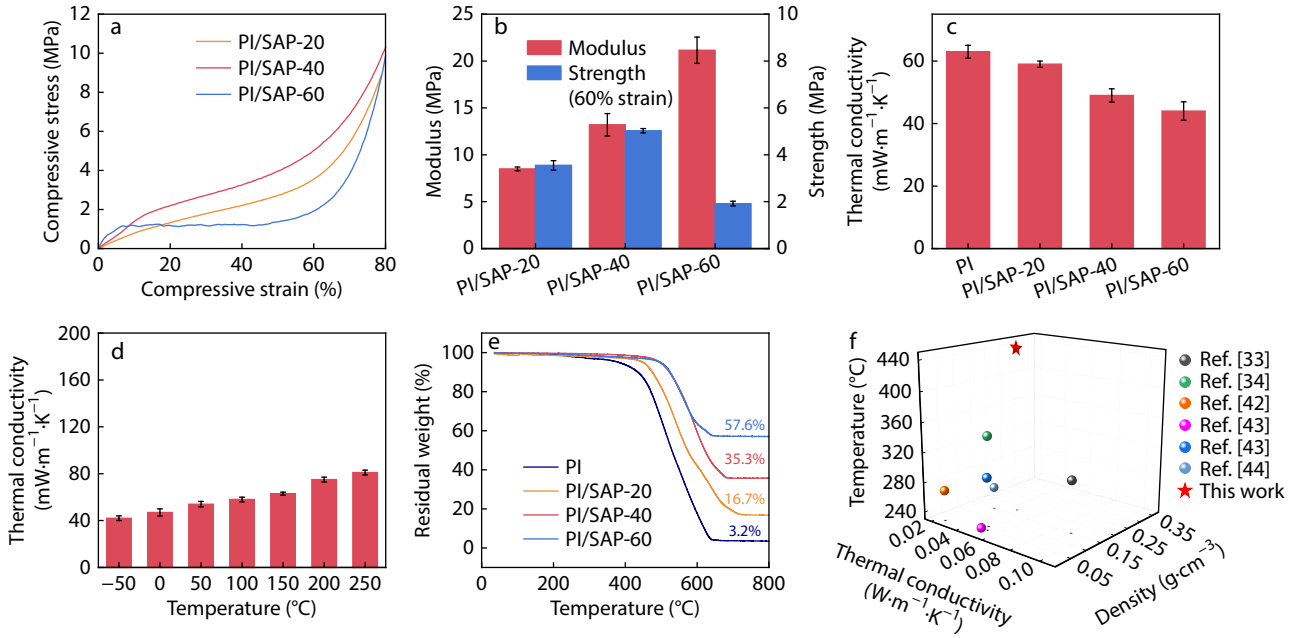

Fig. 3 Mechanical and thermal properties of PI/SAP aerogels. (a) Compressive stress-strain curves of PI/SAP aerogels; (b) Compression modulus and strength of PI/SAP with different SAP contents; (c) Thermal conductivity of PI/SAP aerogels with different SAP contents at room temperature; (d) Thermal conductivity of the PI/SAP-40 aerogel at different temperatures; (e) TGA curves of PI/SAP aerogels under air atmosphere; (f) Comparison of PI/SAP aerogel with other insulation materials in terms of maximum working temperature, density, and thermal conductivity.

https://doi.org/10.1007/s10118-024-3130-8

samples were used for subsequent testing and application. Furthermore, the maximum working temperature, density, and thermal conductivity of PI/SAP aerogel were compared with other 3D printed insulation materials (Fig. 3f), such as polyimide/cellulose nanocrystal composite aerogels,[33] polyimide/bacterial cellulose composite aerogels,[34] carbon nanotubes and carbon nanofibers composite aerogel,[42] cellulose nanofibril aerogel,[43] lignocellulose nanofibril aerogel,[43] and silk fibroin/silica aerogel.[44] The 3D printed PI/SAP aerogels remain thermally stable and well insulated at higher temperatures, suggesting great potential for application in a wide range of temperature environments.

Flame Retardant and Fireproof Characterization of Printed PI/SAP Aerogels

Polyimides are inherently self-extinguishing after leaving the flame. However, when subjected to prolonged flame exposure, they undergo decomposition and carbonization, ultimately leading to the structure collapse of the polyimide aerogel.[45] The addition of inorganic fillers is expected to significantly improve the flame retardancy of the polymers and maintain the stability. As shown in Figs. 4(a)–4(c), combustion experiments were carried out on polystyrene (PS) foam, PI aerogel, and PI/SAP-40 composite aerogel using alcohol lamps, respectively. From the photos, it is obvious that the commercial PS foam burns violently when it contacts with an open flame, and almost burns out finally. Neat PI aerogel is ignited in the flame and carbonized rapidly with a large volume change, and the flame was extinguished by itself after 60 s. In contrast, no obvious flame can be found for PI/SAP-40 after contacting with the flame, and the overall shape and structure did not change obvi-

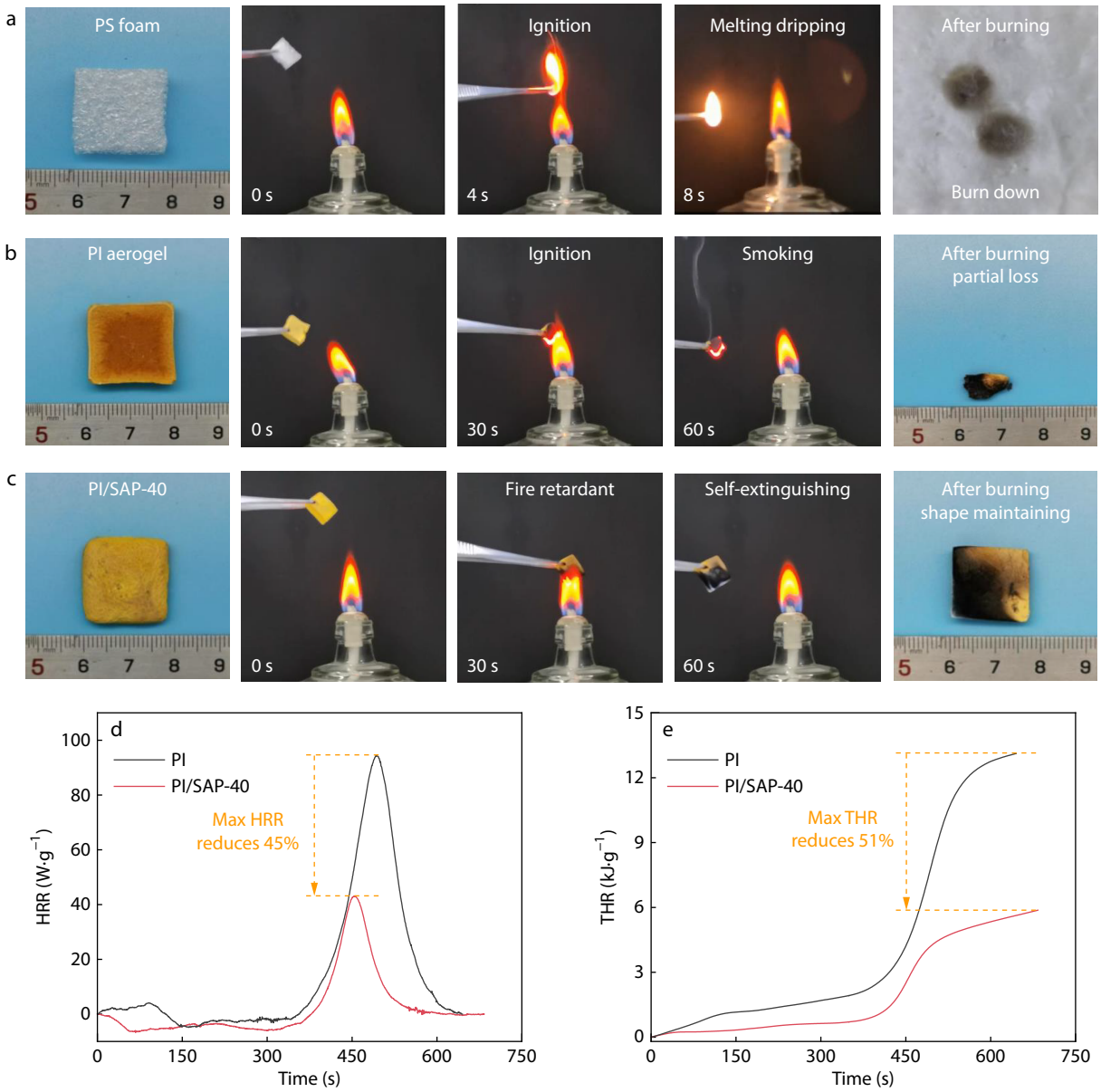

Fig. 4 Flame retardant characterization of printed PI/SAP aerogels. Photography of (a) PS foam, (b) PI aerogel, and (c) PI/SAP-40 aerogels burning by an alcohol burner; (d) Heat release rate (HRR) and (e) total heat release (THR) plots of PI and PI/SAP-40 aerogels.

https://doi.org/10.1007/s10118-024-3130-8

ously, indicating its excellent flame retardant properties. In order to quantitatively characterize the flame retardancy of PI/SAP composite aerogels, we performed a microcalorimetry test on the PI/SAP-40 sample and characterized its heat release rate (HRR), peak heat release peak (pHRR), and total heat release (THR). As shown in Figs. 4(d) and 4(e), PI/SAP-40 exhibits a slower HRR throughout the whole process, and the pHRR value of PI/SAP-40 is only 40.6 $W \cdot g^{-1}$, which is 45% lower than that of neat PI sample. Moreover, the THR value of PI/SAP-40 (6.4 $kJ \cdot g^{-1}$) is much lower than that of PI aerogel (13 $kJ \cdot g^{-1}$), demonstrating the excellent flame retardant performance of PI/SAP composite aerogels. The morphology of PI/SAP-40 composite aerogel after burning was further investigated (Fig. S6 in ESI). Photograph of the PI/SAP-40 aerogel after combustion mainly displays three layers: the white dense layer on the surface, the char layer in the middle, and the unaffected aerogel layer in the back (Figs. S6a and S6b in ESI). The surface layer that in direct contact with the flame was fully burned except SAP, and ultimately only dense silica remained in the surface layer (Fig. S6c in ESI). The remaining dense silica can effectively block the erosion of combustible small molecules and oxygen, protecting the internal structure. Therefore, the porous structure of the char layer is retained (Fig. S6d in ESI), which hinders heat transfer and effectively protects the remaining aerogel body.

Benefiting from the good thermal insulation and flame retardancy, the printed PI/SAP aerogel block is expected to be used for actual fire insulation. As a demonstration, we used a butane blowlamp to test the high-temperature heat insulation performance of the printed PI/SAP aerogel block (Fig. 5a), and the commercial aluminum silicate fireproof felt with the same size (the thickness of 1 cm) was used for comparison. The front surface temperature that in direct contact with flame is about 1289 °C as monitored by an infrared camera (Fig. 5b). The temperature changes on the back of the aluminum silicate felt and PI/SAP-40 within 180 s were recorded by an infrared camera. The back surface temperature of the aluminum silicate felt rises to 290 °C after burning for 60 s and then rises to 377 °C after 180 s (Fig. 5c). In contrast, the back surface temperature of PI/SAP-40 sample only rises to 132 °C after 60 s of burning, and about 298 °C after 180 s (Fig. 5d). The results demonstrate the good heat insulation performance of PI/SAP composite aerogel at high temperature up to ~1300 °C.

3D Printed PI/SAP Aerogel for Battery Insulation

Due to the good thermal insulation performance in a wide

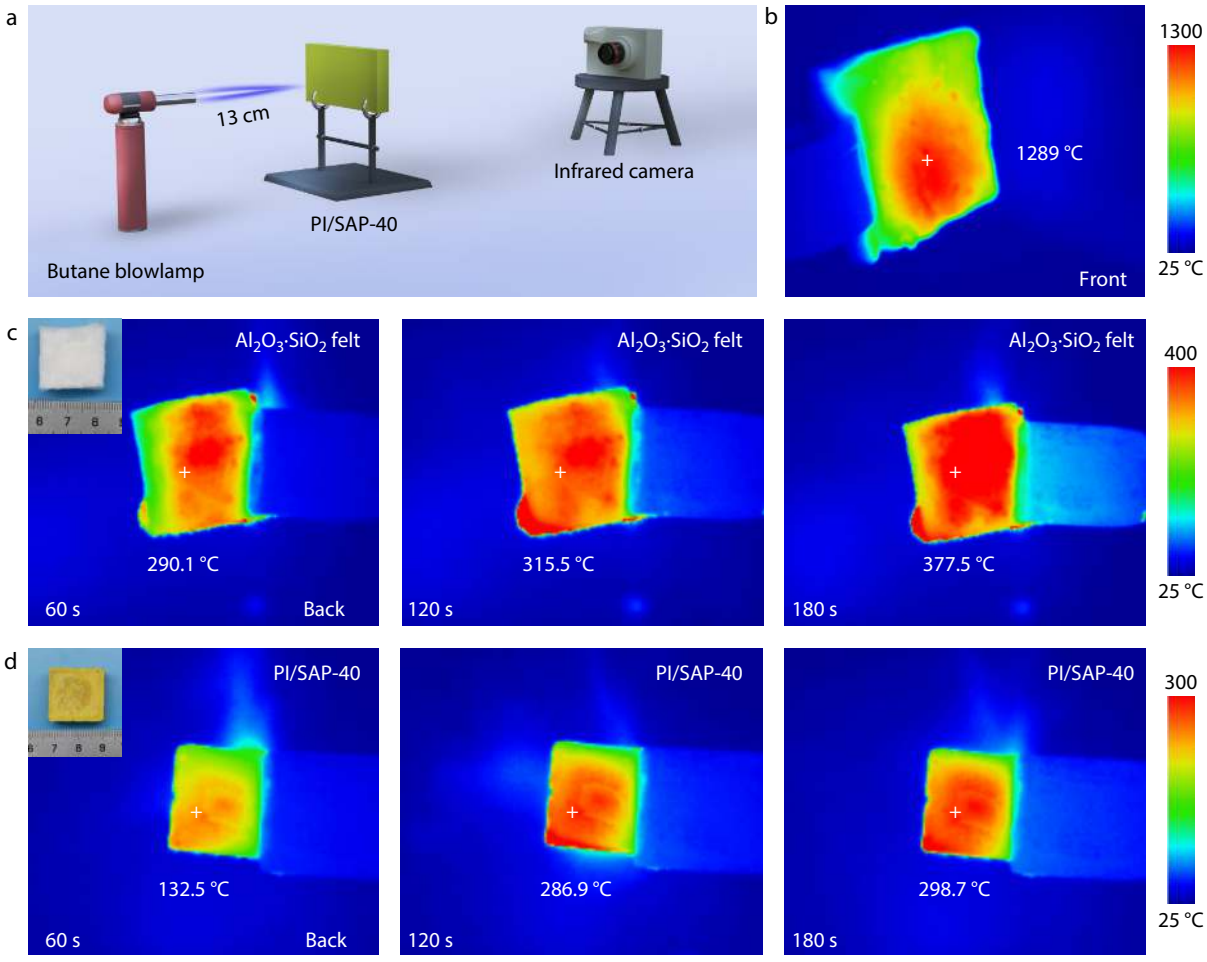

Fig. 5 High-temperature heat insulation performance of PI/SAP aerogel. (a) Diagram of butane blowlamp test. The thickness of samples is 1 cm. (b) Thermal infrared image of burning side; (c) Thermal infrared image of the back side of commercial aluminum silicate fireproof felt; (d) Thermal infrared image of the back side of printed PI/SAP.

https://doi.org/10.1007/s10118-024-3130-8

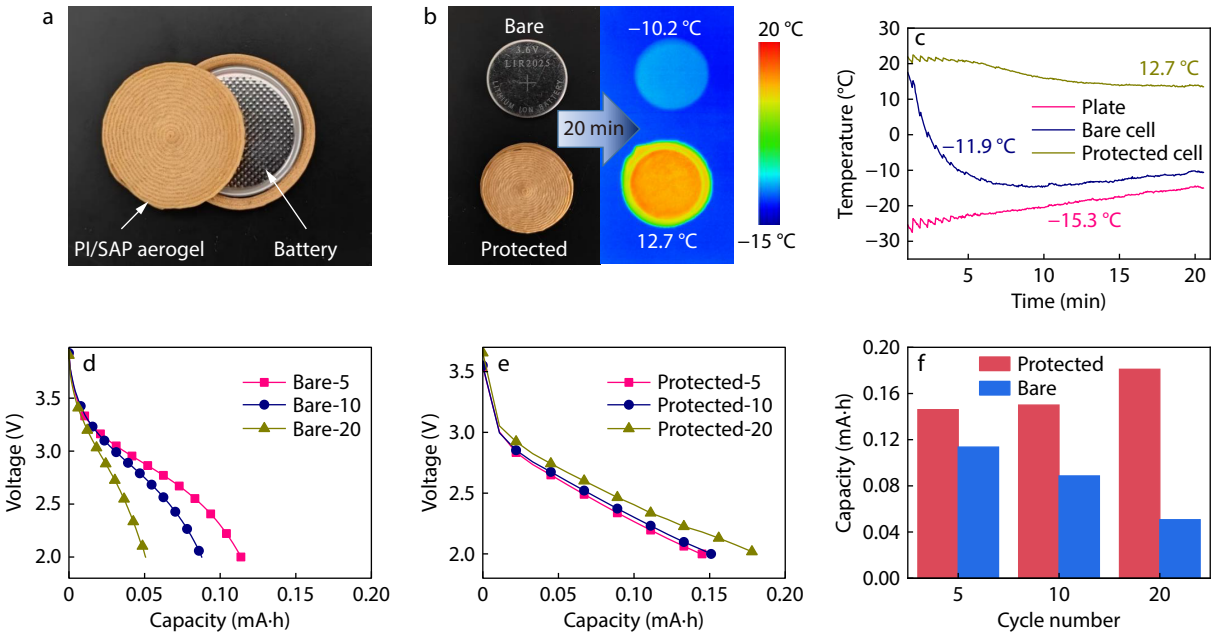

Fig. 6 Battery insulation performance. (a) 3D printed PI/SAP aerogel-based battery protective shell. Commercial ML1220 button cell is used; (b) Photographs and corresponding thermal infrared image of bare and protected batteries on a cold incubator for about 20 min and (c) their surface temperatures over time; Discharge curves of (d) bare and (e) protected cells under −20 °C; (f) The discharge capacity of bare and protected cells under −20 °C.

range of temperatures, the PI/SAP composite aerogel is expected to be applied for thermal insulation for lithium-ion batteries, to improve its capacity in a low-temperature environment. As a proof of concept, a PI/SAP aerogel-based battery protective shell with thickness of about 2 mm was printed according to the size of the battery (commercial ML1220 button cell) (Fig. 6a). Then the battery was placed in the protective shell and placed in a cold incubator together with bare battery for comparison (Fig. 6b). Due to the excellent thermal insulation properties of the PI/SAP aerogel, the temperature of the protected battery was stabilized at 13 °C after 20 min in a −20 °C environment, while the temperature of the unprotected battery decreased rapidly and finally maintained at −15 °C (Fig. 6c). Subsequently, the charge and discharge capacities of the two batteries were tested in the incubator, and the results are shown in Figs. 6(d) and 6(e). Under the temperature of −20 °C, the capacity of the bare battery gradually decreased from 0.12 mA·h at the 5^{th} cycle to 0.05 mA·h at 20^{th} cycle, while the capacity of the protected battery increased from 0.15 mA·h to 0.18 mA·h (Fig. 6f). The slightly increased capacity is probably due to the thermal insulation of PI/SAP that increased the temperature in the insulation shell, which accelerates the ion migration rate in the battery and improves the battery capacity. Therefore, the PI/SAP with customized shape exhibits excellent thermal insulation in subzero-temperature environment, making it easy to be applied to scenes with precise shape requirements.

CONCLUSIONS

In summary, 3D printed PI/SAP composite aerogel with precisely controlled and complex structures has been prepared for good thermal insulation over a wide range of temperatures. The addition of SAP greatly improves the yield stress and modulus of the ink, and effectively inhibits the shrinkage of the 3D printed aerogel products (~14%) to maintain a higher porosity (~92%). The 3D printed PI/SAP composite aerogels can maintain this excellent heat insulation ability in a wide range of temperatures (42 $mW·m^{-1}·K^{-1}$ at −50 °C and 81 $mW·m^{-1}·K^{-1}$ at 250 °C). Moreover, the printed PI/SAP composite aerogels exhibit excellent heat insulation and flame retardant ability and can still maintain their original porous structure under the flame burning at 1300 °C. In addition, the printed PI/SAP composite aerogel as battery protective shell can maintain the capacity of batteries under −20 °C. Therefore, the 3D printed PI/SAP composite aerogels show great potential as a customizable and stable insulating material in a variety of complex and extreme application occasions.

Conflict of Interests

The authors declare no interest conflict.

Electronic Supplementary Information

Electronic supplementary information (ESI) is available free of charge in the online version of this article at http://doi.org/10.1007/s10118-024-3130-8.

Data Availability Statement

The associated data of this article (DOI: 10.57760/sciencedb.j00189.00028) can be accessed from the Science Date Bank database (https://www.scidb.cn/en/s/FBVRfm).

ACKNOWLEDGMENTS

This work was financially supported by the National Key Research and Development Program of China (No. 2022YFB3805700), the National Natural Science Foundation of China (Nos. 52073053 and 52233006), Young Elite Scientists Sponsorship Program by CAST (No. 2021QNRC001), Shanghai Rising-Star Program (No. 21QA1400300), and Innovation Program of Shanghai Municipal Education Commission (No. 2021-01-07-00-03-E00108).

REFERENCES

1 An, L.; Armstrong, J. N.; Hu, Y.; Huang, Y. L.; Li, Z.; Zhao, D. H.; Sokolow, J.; Guo, Z. P.; Zhou, C.; Ren, S. Q. High temperature ceramic thermal insulation material. *Nano Res.* **2022**, *15*, 6662–6669.
2 Wang, Y. T.; Chu, C. Y.; Duan, C. Q.; Dong, J. J.; Chen, H.; Ying, S.; Guo, J.; Xu, G.; Hu, F.; Cheng, Y. Thermal insulation of 3D printed complex and miniaturized SiO_2 aerogels at medium-high temperatures. *J. Non. Cryst. Solids.* **2023**, *608*, 122251.
3 Wu, K. D.; Zhou, Q.; Cao, J. X.; Qian, Z.; Niu, B.; Long, D. H. Ultrahigh-strength carbon aerogels for high temperature thermal insulation. *J. Colloid Interface Sci* **2021**, *609*, 667–675.
4 Tian, J.; Yang, Y.; Xue, T. T.; Chao, G. J.; Fan, W.; Liu, T. X. Highly flexible and compressible polyimide/silica aerogels with integrated double network for thermal insulation and fire-retardancy. *J. Mater. Sci. Technol.* **2021**, *105*, 194–220.
5 Jadhav, P. S.; Sarkar, A.; Pasupathy, S.; Ren, S. Q. Biogenic straw aerogel thermal insulation materials. *Adv. Eng. Mater.* **2023**, *25*, 2300037.
6 Zhang, C. J.; Song, S. C.; Liu, Q.; Li, J. H.; Cao, Q.; Zhang, S. H.; Jian, X. G.; Weng, Z. H. Fabrication of cross-linked polysulfone aerogels for thermal insulation. *Mater. Lett.* **2023**, *351*, 135000.
7 Zou, F. X.; Budtova, T. Polysaccharide-based aerogels for thermal insulation and superinsulation: an overview. *Carbohydr. Polym.* **2021**, *266*, 118130.
8 Coquard, R.; Baillis, D.; Quenard, D. Numerical and experimental study of the IR opacification of polystyrene foams for thermal insulation enhancement. *Energy Build.* **2018**, *183*, 54–63.
9 Ge, C. B.; Zhai, W. T. Cellular thermoplastic polyurethane thin film: preparation, elasticity, and thermal insulation performance. *Ind. Eng. Chem. Res.* **2018**, *57*, 4688–4696.
10 Sair, S.; Mandili, B.; Taqi, M.; Bouari, A. E. Development of a new eco-friendly composite material based on gypsum reinforced with a mixture of cork fibre and cardboard waste for building thermal insulation. *Compos. Commun.* **2019**, *16*, 20–24.
11 Li, M. M.; Chen, X.; Li, X. T.; Dong, J.; Teng, C. Q.; Zhao, X.; Zhang, Q. H. Ultralight aerogel textiles based on aramid nanofibers composites with excellent thermal insulation and electromagnetic shielding properties. *Compos. Commun.* **2022**, *35*, 101346.
12 Wu, Z. H.; Feng, X. L.; Qu, Y. X.; Gong, L. X.; Cao, K.; Zhang, G. D.; Shi, Y. Q.; Gao, J. F.; Song, P. G.; Tang, L. C. Silane modified MXene/polybenzazole nanocomposite aerogels with exceptional surface hydrophobicity, flame retardance and thermal insulation. *Compos. Commun.* **2023**, *37*, 101402.
13 Baetens, R.; Jelle, B. P.; Gustavsen, A. Aerogel insulation for building applications: a state-of-the-art review. *Energy Build.* **2010**, *43*, 761–769.
14 Fan, W.; Zhang, X.; Zhang, Y.; Zhang, Y. F.; Liu, T. X. Lightweight, strong, and super-thermal insulating polyimide composite aerogels under high temperature. *Compos. Sci. Technol* **2019**, *173*, 47–52.
15 Xu, G. F.; Li, M. J.; Wu, T. T.; Teng, C. Q. Highly compressible and anisotropic polyimide aerogels containing aramid nanofibers. *React. Funct. Polym.* **2020**, *154*, 104672.
16 Zhao, S. Y.; Siqueira, G.; Drdova, S.; Norris, D.; Ubert, C.; Bonnin, A.; Sandra Galmarini, S. Additive manufacturing of silica aerogels. *Nature* **2020**, *584*, 387–392.
17 Li, C. D.; Zhang, G. H.; Lin, L. L.; Wu, T. T.; Brunner, S.; Galmarini, S.; Bi, J. T.; J. Malfait, W.; Zhao, S. Y.; Ostrikov, K. Silica aerogels: from materials research to industrial applications. *Int. Mater. Rev.* **2023**, *68*, 862–900.
18 Liu, Z. H.; Ding, Y. D.; Wang, F.; Deng, Z. P. Thermal insulation material based on SiO_2 aerogel. *Constr. Build Mater.* **2016**, *122*, 547–554.
19 Guo, B. F.; Wang, Y. J.; Qu, Z. H.; Yang, F.; Qin, Y. Q.; Li, Y.; Zhang, G. D.; Gao, J. F.; Shi, Y. Q.; Song, P. G.; Tang. L. C. Hydrosilylation adducts to produce wide-temperature flexible polysiloxane aerogel under ambient temperature and pressure drying. *Small* **2023**, *20*, 2309272.
20 Zhang, Z. H.; Chen, Z. Y.; Tang, Y. H.; Li, Y. T.; Zhang, G. D.; Cao, C. F.; Gong, L. X.; Tang, L. C. Silicone/graphene oxide co-cross-linked aerogels with wide-temperature mechanical flexibility, super-hydrophobicity and flame resistance for exceptional thermal insulation and oil/water separation. *J. Mater. Sci. Technol.* **2022**, *114*, 131–142.
21 Zhang, X.; Zhao, X. Y.; Xue, T. T.; Yang, F.; Fan, W.; Liu, T. X. Bidirectional anisotropic polyimide/bacterial cellulose aerogels by freeze-drying for super-thermal insulation. *Chem. Eng. J.* **2019**, *385*, 123963.
22 Fraleoni-Morgera, A.; Chhikara, M. Polymer-based nano-composites for thermal insulation. *Adv. Eng. Mater.* **2019**, *21*, 1801162.
23 Zhao, W.; Zhu, J.; Liu, L. W.; Leng, J. S.; Liu, Y. J. A bio-inspired 3D metamaterials with chirality and anti-chirality topology fabricated by 4D printing. *Int. J. Smart Nano Mater.* **2023**, *14*, 1–20.
24 Jiang, Y. Q.; Xu, Z.; Huang, T. Q.; Liu, Y. J.; Guo, F.; Xi, J. B.; Gao, W. W.; Gao, C. Direct 3D printing of ultralight graphene oxide aerogel microlattices. *Adv. Funct. Mater.* **2018**, *28*, 1707024.
25 Joo, P.; Yao, Y.; Teo, N.; Jana, S. C. Modular aerogel brick fabrication *via* 3D-printed molds. *Addit. Manuf.* **2021**, *46*, 102069.
26 Zhang, Q. Q.; Zhang, F.; Medarametla, S. P.; Li, H.; Zhou, C.; Lin, D. 3D printing of graphene aerogels. *Small* **2016**, *12*, 1702–1708.
27 Cheng, Q. Q.; Sheng, Z. Z.; Wang, Y. F.; Lyu, J.; Zhang, X. T. General suspended printing strategy toward programmatically spatial Kevlar aerogels. *ACS Nano* **2022**, *16*, 4905–4916.
28 Chen, N.; Luo, F. Y.; Yang, G. W.; Yao, J. R.; Chen, X.; Shao, Z. Z. Production of functional materials derived from regenerated silk fibroin by utilizing 3D printing and biomimetic enzyme-induced mineralization. *Chinese J. Polym. Sci.* **2023**, *42*, 299–310.
29 Ching, T.; Li, Y. Y.; Karyappa, R.; Ohno, A.; Toh, Y. C.; Hashimoto, M. Fabrication of integrated microfluidic devices by direct ink writing (DIW) 3D printing. *Sens. Actuators B Chem.* **2019**, *297*, 126609.
30 Guan, R. H.; Zheng, H. Y.; Liu, Q. X.; Ou, K. T.; Li, D. S.; Fan, J.; Fu, Q.; Sun, Y. Y. DIW 3D printing of hybrid magnetorheological materials for application in soft robotic grippers. *Compos. Sci. Technol.* **2022**, *223*, 109409.
31 Yang, G. Y.; Sun, Y. Y.; Qin, L. M.; Li, M. R.; Ou, K. T.; Fang, J.; Fu, Q. Direct-ink-writing (DIW) 3D printing functional composite materials based on supra-molecular interaction. *Compos. Sci. Technol.* **2021**, *215*, 109013.
32 Yang, G. Y.; Guan, R. H.; Zhen, H. Y.; Ou, K. T.; Fang, J.; Li, D. S.; Fu, Q.; Sun, Y. Y. Tunable size of hierarchically porous alumina ceramics based on DIW 3D printing supramolecular gel. *ACS Appl. Mater. Interfaces* **2022**, *14*, 10998–11005.

https://doi.org/10.1007/s10118-024-3130-8

33 Feng, C. A.; Yu, S. S. 3D printing of thermal insulating polyimide/cellulose nanocrystal composite aerogels with low dimensional shrinkage. *Polymers* **2021**, *13*, 3614.

34 Ma, Z. C.; Xue, T. T.; Wali, Q.; Miao, Y. E.; Fan, W.; Liu, T. X. Direct ink writing of polyimide/bacterial cellulose composite aerogel for thermal insulation. *Compos. Commun.* **2023**, *39*, 101528.

35 Wu, T. T.; Ganobjak, M.; Siqueira, G.; Zeng, Z. H.; Li, M. M.; Filimonova, E.; Saghamanesh, S.; Bonnin, A.; Sivaraman, D.; Yip, J.; Li, L.; Wu, H.; Nyström, G.; Malfalt, W. J.; Zhao, S. 3D printed polyimide nanocomposite aerogels for electromagnetic interference shielding and thermal management. *Adv. Mater. Technol.* **2023**, *8*, 2202155.

36 Xue, T. T.; Yang, Y.; Yu, D. Y.; Wali, Q.; Wang, Z. Y.; Cao, X. S.; Fan, W.; Liu, T. X. 3D printed integrated gradient-conductive MXene/CNT/polyimide aerogel frames for electromagnetic interference shielding with ultra-low reflection. *Nano-Micro Lett.* **2023**, *15*, 45.

37 Yang, Y.; Fan, W.; Yuan, S. J.; Tian, J.; Chao, G. J.; Liu, T. X. A 3D-printed integrated MXene-based evaporator with a vertical array structure for salt-resistant solar desalination. *J. Mater. Chem. A* **2021**, *9*, 23968–23976.

38 Zhang, T. T.; Zhou, M. X.; Guo, Z. Y.; Zhao, Y. B.; Han, D.; Xiu, H.; Bai, H. W.; Zhang, Q.; Fu, Q. Improving impact toughness of polylactide/ethylene-*co*-vinyl-acetate blends *via* adding fumed silica nanoparticles: effects of specific surface area-dependent interfacial selective distribution of silica. *Chinese J. Polym. Sci.* **2021**, *39*, 1040–1049.

39 Chen, Q. F.; Wang, H.; Sun, L. Y. Preparation and characterization of silica aerogel microspheres. *Materials* **2017**, *10*, 435.

40 Peng, T. P.; Zhu, J. D.; Huang, T.; Jiang, C. W.; Zhao, F. X.; Ge, S. Z.; Xie, L. Facile preparation for gelatin/hydroxyethyl cellulose-SiO_2 composite aerogel with good mechanical strength, heat insulation, and water resistance. *J. Appl. Polym. Sci.* **2021**, *138*, e50539.

41 Babiarczuk, B.; Lewandowski, D.; Szczurek, A.; Kierzek, K.; Meffert, M.; Gerthsen, D.; Kaleta, J.; Krzak, J. Novel approach of silica-PVA hybrid aerogel synthesis by simultaneous sol-gel process and phase separation. *J. Supercrit. Fluids* **2020**, *166*, 104997.

42 Wang, F.; Yang, Z. J.; Hu, X. Z.; Pan, Y.; Lu, Y.; Jiang, M. Coaxial 3D printed anisotropic thermal conductive composite aerogel with aligned hierarchical porous carbon nanotubes and cellulose nanofibers. *Smart Mater. Struct.* **2022**, *31*, 045002.

43 Liu, C. H.; Li, M. C.; Liu, X. Y.; Zhou, G. Q.; Liu, C. Z.; Mei, C. T. 3D printing of customized lignocellulose nanofibril aerogels for efficient thermal insulation. *Addit. Manuf.* **2023**, *78*, 103841.

44 Maleki, H.; Montes, S.; Hayati-Roodbari, N.; Putz, F.; Huesing, N. Compressible, thermally insulating, and fire retardant aerogels through self-assembling silk fibroin biopolymers inside a silica structure—an approach towards 3D printing of aerogels. *ACS Appl. Mater. Interfaces* **2018**, *10*, 22718.

45 Wang, Y. J.; Cui, Y.; Shao, Z. Y.; Gao, W. W.; Fan, W.; Liu, T. X.; Bai, H. Multifunctional polyimide aerogel textile inspired by polar bear hair for thermoregulation in extreme environments. *Chem. Eng. J.* **2020**, *390*, 124623.

https://doi.org/10.1007/s10118-024-3130-8